Adsorption isotherms and thermal behavior of hybrids based on quercetin and inorganic fillers

Azzurra Milia,[1] Maurizio Bruno,[1] Giuseppe Cavallaro,[2*] Giuseppe Lazzara,[2,3] Stefana Milioto[2,3]

[1]Dipartimento STEBICEF, Università degli Studi di Palermo, Viale delle Scienze, pad. 17, 90128 Palermo, Italy.

[2]Dipartimento di Fisica e Chimica, Università degli Studi di Palermo, Viale delle Scienze, pad. 17, 90128 Palermo, Italy.

[3]Consorzio Interuniversitario Nazionale per la Scienza e Tecnologia dei Materiali, INSTM, Via G. Giusti, 9, I-50121 Firenze, Italy

*giuseppe.cavallaro@unipa.it

Abstract

We investigated the adsorption process of quercetin onto several inorganic fillers, such as kaolinite, calcium carbonate and alumina. Firstly, we performed equilibrium adsorption studies in order to determine the quercetin/filler adsorption isotherms, which were successfully fitted through the Langmuir model. Based on the adsorption data analysis, we estimated the maximum adsorption capacity of each filler as well as the Langmuir constant, which is related to the affinity between quercetin and the surfaces of the inorganic particles. Then, we prepared hybrids formed by fillers saturated with quercetin. The obtained composites were characterized by thermogravimetric (TG) analysis with the aim to determine the loading efficiency as well as the effect of the adsorption process on the quercetin thermal stability. According to the Langmuir isotherms, alumina revealed the most efficient support for quercetin adsorption. Finally, we observed that the interactions with the fillers' surfaces induce a reduction of the quercetin degradation temperature.

Keywords: Thermogravimetry, Adsorption isotherms, Quercetin, Kaolinite, Alumina, Calcium Carbonate

Introduction

In the last decades, inorganic particles have been proposed as fillers for numerous applications within catalysis [1,2]. biotechnology [3,4], packaging [5,6], remediation [7–9] and restoration [10–12]. The adsorption onto the filler surfaces represents an efficient strategy to obtain drug delivery systems with controlled loading and release properties [13,14].

In this regard, clay nanoparticles are suitable nanocarriers because of their peculiar layered structure that can favor the entrapment of biologically and chemically active molecules [15]. Among the clay minerals, kaolinite is the most abundant worldwide. Kaolinite belongs to the 1:1 phyllosilicates group being that the component layers are formed by one octahedral sheet of alumina and one tetrahedral sheet of silica. Kaolinite possesses a platy morphology with a low specific surface area (around 8–15 m^2 g^{-1}). As evidenced by a recent review [16], kaolinite clay can be employed as pharmaceutical excipient due to its capacity to control the release of functional components in drug administration and delivery. The rolling of kaolinite sheets generates clay nanotubes that can incorporate guest molecules (antimicrobial [17], antioxidant [18] and anticorrosive [19] compounds) within their cavity allowing to extend their action time. Kaolinite particles can be used as removal agents for wastewater remediation as a consequence of their ability to adsorb heavy metals [20,21] and organic pollutants [22]. Moreover, kaolinite revealed as effective adsorbent for dyes, such as Brilliant Green [23], Neutral Red [24], Rhodamine 6G [8] and Chrome azurol S [8].

Calcium carbonate ($CaCO_3$) particles were successfully employed as mesoporous inorganic fillers for dyes adsorption as proved for Congo Red [25] and photoditazine [26]. An efficient coating pigment can be achieved using $CaCO_3$ particles with 0.4-2 μm size range and a specific surface area of 4–11 m^2 g^{-1} [27]. $CaCO_3$ fillers are natural materials obtained mostly from limestone. This mineral can exhibit three different crystal polymorphs (rhombohedral, orthorhombic and hexagonal), which affect the morphological characteristics of the $CaCO_3$ particles and, consequently, their adsorption capacities. $CaCO_3$ particles are commonly used as fillers for polymer matrix. Literature [28] reports that the addition of $CaCO_3$ into polypropylene caused an

enhancement of the mechanical properties of the polymer. Polycaprolactone/chitosan blend filled with $CaCO_3$ particles showed an improvement of both the mechanical performance and the thermal stability [29].

Among nanofillers for engineering and technological applications, alumina (Al_2O_3) is an emerging material because of its morphological characteristics and tunable surface properties. The synthesis of Al_2O_3 particles can be achieved by means of different procedures, such as sol-gel preparation [30] and selective corrosion combined with coagulation separation [31]. The preparation procedures affect the geometrical characteristics of alumina. Al_2O_3 nanorods with a length of 150 nm and a diameter of ca. 15 nm in length were prepared by calcination of fine boehmite powders at 1000 °C [32]. The synthesis of alumina particles with a specific surface area of 150 m^2 g^{-1} were obtained by the dehydration of diaspore to Al_2O_3 [33]. Activated alumina particles revealed as efficient adsorbent for heavy metals [34], hydrocarbons [35] and textile dyes, such as Alizarin Red S and Cibacron reactive yellow [36]. Alumina can be employed as reinforcing nanofiller for polymers as demonstrated in the nanocomposites based on Poly(methyl methacrylate) [37].

Here, we studied the adsorption capacities of the mentioned fillers (kaolinite, calcium carbonate and alumina) towards quercetin, which is a natural yellow dye with anticancer [38] and antioxidant [39] activities. Quercetin is a flavonol (3-hydroxy flavones) that can be obtained by different plants including Persian berries (*Rhamnus* spp.), young fustic (*Cotinus coggygria*), old fustic (*Chlorophora tinctoria*) and yellow wood (*Solidago virgaurea*). The encapsulation of quercetin within clay nanotubes as well as pluronic nanoparticles was successfully conducted allowing to extend the functionality of the molecule. Accordingly, the quercetin/nanoparticle systems revealed as promising carriers for medical treatments (as demonstrated for thyroid cancer cells [40]) and fabrication of photo-oxidative resistant materials [41].

In conclusion, this work was aimed to investigate the quercetin adsorption onto inorganic fillers. The quercetin/filler systems might be promising as functional nanocarriers on dependence of their composition, which was investigated by both equilibrium adsorption isotherms and

thermogravimetry (TG). Accordingly to the recent literature, thermogravimetric analysis represents an efficient and robust method to investigate multicomponent materials [10,42–47] and dyes [48]. Within this, the analysis and interpretation of TG curves can provide a direct relation between the thermal behavior of composites and their corresponding composition [10]. On this basis, the thermal characteristics of quercetin/fillers systems were correlated to the corresponding adsorption isotherms driving to evaluate the perspectives of the hybrids.

Experimental

Materials

Ethanol, Quercetin (Q), Kaolinite (Kao), activated basic Alumina (Al_2O_3) and Calcium Carbonate ($CaCO_3$) are from Sigma Aldrich. All the products were used without any further purification.

Loading of quercetin onto the inorganic fillers

Quercetin was loaded onto the fillers by ethanol solution using a typical procedure employed for the preparation of drug/filler carriers [17]. Firstly, we prepared 100 mL of saturated quercetin solution in ethanol (the concentration was 2 mg mL^{-1}). Then, 2 grams of the fillers were added to the quercetin solution and the obtained dispersion was magnetically stirred for 48 h at 25 °C. Successively, the dispersion was centrifuged to recover the quercetin/filler material. The latter was washed with ethanol three times in order to avoid the presence of free quercetin in the composite. Finally, the solid material was dried at 35 °C to evaporate the solvent and stored in a desiccator at 25 °C. The described procedure was separately conducted for the quercetin loading onto kaolinite, calcium carbonate and alumina.

Methods

Spectrophotometry

Spectrophotometric experiments were conducted to investigate the equilibrium adsorption isotherms, which provide the adsorption capacities of the fillers (kaolinite, alumina and calcium carbonate) towards quercetin. The experiments were carried out using an Analytik Jena Specord S600 BU in isothermal conditions (the temperature was set at 25.0±0.1 °C). The ethanol solution of quercetin exhibits the maximum of the absorption band at 372 nm with a specific extinction coefficient of 2.99 mL g^{-1} cm^{-1}. To this purpose, quercetin/filler dispersions were prepared and equilibrated for 48 hours. The cocentration of quercetin was kept constant (0.5 g mL^{-1}), while the content of fillers was systematically changed. Then, the absorbance of quercetin in the supernatant was measured. The percent of the adsorbed quercetin was estimated by the following equation:

$$A\% = 10^2 \cdot (C_{Qi} - C_{Qf})/(C_{Qi}) \quad (1)$$

where C_{Qi} is the initial concentration of the quercetin solution, while C_{Qf} corresponds to the concentration of quercetin in the supernatant after the equilibration with the fillers.

Thermogravimetry (TG)

The measurements were performed using a Q5000 IR apparatus (TA Instruments) under a nitrogen flow of 25 cm^3 min^{-1} for the sample and 10 cm^3 min^{-1} for the balance. The samples (ca. 5 mg) were heated from 25 to 600 °C. The heating rate was set at 20 °C min^{-1}. TG analyses were performed on the fillers loaded with quercetin as well as on the corresponding pristine components. The temperature calibration of the apparatus was conducted on the basis of the Curie temperatures of standards (nickel, cobalt, and their alloys).

Results

Equilibrium adsorption isotherms

Equilibrium adsorption studies were conducted on quercetin/filler mixtures with variable composition. Some examples of the dispersions after the equilibration are displayed in Figure 1a, which shows the clear separation between the supernatant (ethanol phase) and the sediment (filler). Kaolinite and $CaCO_3$ particles did not completely adsorb quercetin as evidenced by the supernatants, which are yellow colored because of the presence of the dye. Contrarily, the ethanol phase on alumina sediment is transparent. Figure 1b shows the dependence of the adsorption efficiency (expressed as percent of adsorbed quercetin) on the concentration of the fillers in the ethanol dispersions.

As a general result, the increase of the adsorbent concentration generated an enhancement of the adsorption efficiency, which approaches to a constant value as a consequence of the saturation of the fillers' surfaces. Interestingly, alumina acted as the most efficient adsorbent being that its adsorption efficiency is almost equals to 100%, while A% values for the saturated kaolinite and $CaCO_3$ fillers are ca. 25 and 40%, respectively.

The adsorption isotherms were successfully analyzed by using the Langmuir model, which provides the maximum adsorption capacity (Q_{max}) as well as the adsorption constant (K_{ads}) based on the equation

$$(Q_e)^{-1} = (Q_{max} \cdot K_{ads} \cdot C_e)^{-1} + (Q_{max})^{-1} \quad (2)$$

where C_e represents the quercetin concentration in solution, and Q_e is the equilibrium adsorbent capacity, which can be calculated as

$$Q_e = (C_{Qi} - C_{Qf})/C_{ads} \quad (3)$$

being C_{ads} the concentration of the adsorbent fillers in the ethanol dispersion.

According to the equation 2, the $(Q_e)^{-1}$ vs $(C_e)^{-1}$ plots exhibited a linear trend for all the investigated systems (Figure 2) highlighting that the Langmuir model is appropriate for the description of the

quercetin adsorption onto the fillers. Table 1 collects the adsorption parameters obtained by the Langmuir fitting for the quercetin/fillers systems.

Table 1. Adsorption isotherm parameters obtained by the Langmuir model.

filler	Q_{max} / g_Q g_{ads}^{-1}	K_{ads} / mL g_Q^{-1}
Kaolinite	0.14 ± 0.03	46 ± 2
Calcium Carbonate	0.11 ± 0.04	75.1 ± 1.2
Alumina	0.18 ± 0.05	460 ± 60

As concerns the adsorption constant, we detected that K_{ads} of alumina is ca 1 order larger than those of the other investigated fillers. This finding reflects the strongest affinity of quercetin towards alumina surfaces. Moreover, alumina possesses the largest Q_{max} value in agreement with its most efficient adsorption capacity. The latter can be attributed to the largest specific surface area of alumina particles.

Thermal characterization of quercetin/fillers systems

Thermogravimetry experiments were performed on the quercetin/filler composites and their pure components with the aim to investigate 1) the quercetin loading onto the fillers' surfaces; 2) the effect of the adsorption on the quercetin thermal behavior. As shown by Figure 3, quercetin presents two degradation steps occurring in the temperature ranges between 120-180 and 200-400 °C with mass losses of 10.4 and 49.3 wt%, respectively.The absence of mass loss from 25 to 120 °C highlighted that quercetin is an anhydrous material, while the residual mass at 700 °C (20.3 %) evidenced that the quercetin thermal decomposition is not complete even at very high temperature.

Figure 4 compares the TG curves of the quercetin/filler hybrids with those of the pure particles.

Due to the quercetin adsorption, the composite materials possess lower residual masses at 700 °C with respect to those of the corresponding pure fillers. As reported elsewhere [49], the percent of

quercetin loaded on the fillers (Table 2) was estimated by the quantitative analysis of the TG data using the rule of mixtures on the residual masses at 700 °C.

Table 2. Quercetin loading determined by Thermogravimetry

filler	Loading / wt%
Kaolinite	1.53 ± 0.07
Calcium Carbonate	10.3 ± 0.5
Alumina	20.4 ± 1.2

According to the adsorption isotherms fitting, the largest quercetin loading was detected for alumina fillers. It should be noted that the loadings calculated from TG data are in agreement with the Q_{max} values (Table 1) for both alumina and calcium carbonate. On the contrary, the percent of quercetin adsorbed on kaolinite (Table 2) is underestimated compared with that expected by the corresponding Q_{max} value (Table 1).

The influence of the adsorption on the quercetin thermal behavior was explored by focusing on the degradation step at 200-400 °C being that most of quercetin decomposes within this temperature interval (Figure 3). The differential thermogravimetric (DTG) curve of quercetin (Figure 5) shows a single peak centered at 353.8 °C.

We observed that the DTG peak is shifted to lower temperature for all the quercetin/filler hybrids (Figure 6) highlighting the thermal destabilization induced by the quercetin adsorption onto the fillers' surfaces. Table 3 collects the quercetin degradation temperatures determined from the DTG peak minima. Interestingly, the strongest destabilization effect on the quercetin thermal decomposition was observed for alumina, which exhibited the highest affinity and adsorption capacity. The thermal results of the hybrids could be related to specific surface area of each nanofillers. Specifically, alumina induced the strongest catalytic effect on the quercetin thermal degradation in agreement with its largest specific surface.

Table 3. Quercetin degradation temperature determined from DTG peaks.

Material	Quercetin degradation temperature / °C
Quercetin	353.8
Quercetin/Kaolinite	320.0
Quercetin/Calcium Carbonate	308.9
Quercetin/Alumina	270.8

Conclusions

Hybrid materials based on quercetin and several fillers (kaolinite, calcium carbonate and alumina) were investigated by equilibrium adsorption studies and thermogravimetry. The equilibrium adsorption isotherms were successfully fitted by the Langmuir model, which evidenced that alumina particles possess the strongest affinity and adsorption capacity towards quercetin. Interestingly, the adsorption constant for quercetin/alumina is one order larger than those of quercetin/kaolinite and quercetin/calcium carbonate systems. The quantitative analysis of the thermogavimetric data highlighted that the largest quercetin loading is achieved in the composites based on alumina fillers confirming the equilibrium adsorption isotherms. In general, the adsorption process generated a decrease of the quercetin degradation temperature. The strongest thermal destabilization (ca. 80 °C) was detected in the quercetin/alumina composites.

Acknowledgments

The authors acknowledge the financial supports from Progetto di ricerca e sviluppo "AGM for CuHe (ARS01_00697)" and University of Palermo.

References

1. Cattaneo AS, Ferrara C, Marculescu AM, Giannici F, Martorana A, Mustarelli P, et al. Solid-state NMR characterization of the structure and thermal stability of hybrid organic–inorganic compounds based on a HLaNb2O7 Dion–Jacobson layered perovskite. Phys Chem Chem Phys. 2016;18:21903–12.

2. Groppo E, Agostini G, Borfecchia E, Lazzarini A, Liu W, Lamberti C, et al. The Pyridyl Functional Groups Guide the Formation of Pd Nanoparticles Inside A Porous Poly(4-Vinyl-Pyridine). ChemCatChem. 2015;7:2188–95.

3. Cavallaro G, Lazzara G, Milioto S, Parisi F, Evtugyn V, Rozhina E, et al. Nanohydrogel Formation within the Halloysite Lumen for Triggered and Sustained Release. ACS Appl Mater Inter. 2018;10:8265–73.

4. Catauro M, Naviglio D, Risoluti R, Vecchio Ciprioti S. Sol–gel synthesis and thermal behavior of bioactive ferrous citrate–silica hybrid materials. J Therm Anal Calorim. 2018;133:1085–92.

5. Soares NFF, Moreira FKV, Fialho TL, Melo NR. Triclosan-based antibacterial paper reinforced with nano-montmorillonite: a model nanocomposite for the development of new active packaging. Polym Advan Technol. 2012;23:901–8.

6. Gorrasi G, Pantani R, Murariu M, Dubois P. PLA/Halloysite Nanocomposite Films: Water Vapor Barrier Properties and Specific Key Characteristics. Macromol Mater Eng. 2014;299:104–15.

7. Junior CRF, Tanaka FN, Bortolin A, de Moura MR, Aouada FA. Thermal and morphological characterization of highly porous nanocomposites for possible application in potassium controlled release. J Therm Anal Calorim. 2018;131:2205–12.

8. Zhao Y, Abdullayev E, Vasiliev A, Lvov Y. Halloysite nanotubule clay for efficient water purification. J Colloid Interf Sci. 2013;406:121–9.

9. Lee J, Ko J, Ryu J, Shin J, Kim H, Sohn D. Catechol grafted silica particles for enhanced adhesion to metal by coordinate bond. Colloids Surf A Physicochem Eng Asp. 2016;511:55–63.

10. Cavallaro G, Milioto S, Parisi F, Lazzara G. Halloysite Nanotubes Loaded with Calcium Hydroxide: Alkaline Fillers for the Deacidification of Waterlogged Archeological Woods. ACS Appl Mater Inter. 2018;10:27355–64.

11. Cavallaro G, Lazzara G, Milioto S, Parisi F. Halloysite nanotubes as sustainable nanofiller for paper consolidation and protection. J Therm Ana.l Calorim. 2014;117:1293–8.

12. Poggi G, Toccafondi N, Melita LN, Knowles JC, Bozec L, Giorgi R, et al. Calcium hydroxide nanoparticles for the conservation of cultural heritage: new formulations for the deacidification of cellulose-based artifacts. Appl Phys A. 2014;114:685–93.

13. Joshi A, Abdullayev E, Vasiliev A, Volkova O, Lvov Y. Interfacial Modification of Clay Nanotubes for the Sustained Release of Corrosion Inhibitors. Langmuir. 2013;29:7439–48.

14. Elumalai DN, Tully J, Lvov Y, Derosa PA. Simulation of stimuli-triggered release of molecular species from halloysite nanotubes. J App Phys. 2016;120:134311.

15. Lazzara G, Cavallaro G, Panchal A, Fakhrullin R, Stavitskaya A, Vinokurov V, et al. An assembly of organic-inorganic composites using halloysite clay nanotubes. Curr Opin Colloid Interface Sci. 2018;35:42–50.

16. Awad ME, López-Galindo A, Setti M, El-Rahmany MM, Iborra CV. Kaolinite in pharmaceutics and biomedicine. Int J Pharmaceut. 2017;533:34–48.

17. Makaremi M, Pasbakhsh P, Cavallaro G, Lazzara G, Aw YK, Lee SM, et al. Effect of Morphology and Size of Halloysite Nanotubes on Functional Pectin Bionanocomposites for Food Packaging Applications. ACS Appl Mater Inter. 2017;9:17476–88.

18. Zhong B, Lin J, Liu M, Jia Z, Luo Y, Jia D, et al. Preparation of halloysite nanotubes loaded antioxidant and its antioxidative behaviour in natural rubber. Polym Degrad Stab. 2017;141:19–25.

19. Fix D, Andreeva DV, Lvov YM, Shchukin DG, Möhwald H. Application of Inhibitor-Loaded Halloysite Nanotubes in Active Anti-Corrosive Coatings. Adv Funct Mater. 2009;19:1720–7.

20. Zhu H, Xiao X, Guo Z, Han X, Liang Y, Zhang Y, et al. Adsorption of vanadium (V) on natural kaolinite and montmorillonite: Characteristics and mechanism. App Clay Sci. 2018;161:310–6.

21. Liu X, Hicher P, Muresan B, Saiyouri N, Hicher P-Y. Heavy metal retention properties of kaolin and bentonite in a wide range of concentration and different pH conditions. App Clay Sci. 2016;119:365–74.

22. Zhang Q, Yan Z, Ouyang J, Zhang Y, Yang H, Chen D. Chemically modified kaolinite nanolayers for the removal of organic pollutants. App Clay Sci. 2018;157:283–90.

23. Nandi BK, Goswami A, Purkait MK. Adsorption characteristics of brilliant green dye on kaolin. J Hazard Mater. 2009;161:387–95.

24. Luo P, Zhao Y, Zhang B, Liu J, Yang Y, Liu J. Study on the adsorption of Neutral Red from aqueous solution onto halloysite nanotubes. Water Res. 2010;44:1489–97.

25. Chong KY, Chia CH, Zakaria S, Sajab MS. Vaterite calcium carbonate for the adsorption of Congo red from aqueous solutions. J Environ Chem Eng. 2014;2:2156–61.

26. Vantsyan MA, Kochetkov AA, Marchenko IV, Kiryukhin YI, Nabatov BV, Artemov VV, et al. Nanostructured calcium carbonate particles as fluorophore carriers. Cryst Rep. 2015;60:951–8.

27. Al Omari MMH, Rashid IS, Qinna NA, Jaber AM, Badwan AA. Chapter Two - Calcium Carbonate. In: Brittain HG, editor. Profiles of Drug Substances, Excipients and Related Methodology. Academic Press; 2016. p. 31–132.

28. Thenepalli T, Jun AY, Han C, Ramakrishna C, Ahn JW. A strategy of precipitated calcium carbonate (CaCO3) fillers for enhancing the mechanical properties of polypropylene polymers. Korean J Chem Eng. 2015;32:1009–22.

29. Abdolmohammadi S, Siyamak S, Ibrahim NA, Yunus WMZW, Rahman MZA, Azizi S, et al. Enhancement of Mechanical and Thermal Properties of Polycaprolactone/Chitosan Blend by Calcium Carbonate Nanoparticles. Int J Mol Sci. 2012;13:4508–4522.

30. Hao Z, Liu H, Guo B, Li H, Zhang J, Gan L, et al. Sol-Gel Synthesis of Alumina Using Inorganic Salt Precursor. Acta Chim Sinica. 2007;23:289–94.

31. Pu S, Li L, Ma J, Lu F, Li J. Disperse fine equiaxed alpha alumina nanoparticles with narrow size distribution synthesised by selective corrosion and coagulation separation. Sci Rep. 2015;5:11575–11575.

32. Zhang X, Ge Y, Hannula S-P, Levänen E, Mäntylä T. Nanocrystalline α-alumina with novel morphology at 1000 °C. J Mater Chem. 2008;18:2423–5.

33. McHale JM, Navrotsky A, Perrotta AJ. Effects of Increased Surface Area and Chemisorbed H2O on the Relative Stability of Nanocrystalline γ-Al2O3 and α-Al2O3. J Phys Chem B. 1997;101:603–13.

34. Naiya TK, Bhattacharya AK, Das SK. Adsorption of Cd(II) and Pb(II) from aqueous solutions on activated alumina. J Colloid Interf Sci. 2009;333:14–26.

35. Díaz E, Ordóñez S, Vega A, Coca J. Adsorption characterisation of different volatile organic compounds over alumina, zeolites and activated carbon using inverse gas chromatography. J Chromatogr A. 2004;1049:139–46.

36. Wasti A, Ali Awan M. Adsorption of textile dye onto modified immobilized activated alumina. J Assoc Arab Univ Basic Appl. 2016;20:26–31.

37. Alzarrug FA, Dimitrijević MM, Jančić Heinemann RM, Radojević V, Stojanović DB, Uskoković PS, et al. The use of different alumina fillers for improvement of the mechanical properties of hybrid PMMA composites. Mater Des. 2015;86:575–81.

38. Zhou J, Fang L, Liao J, Li L, Yao W, Xiong Z, et al. Investigation of the anti-cancer effect of quercetin on HepG2 cells in vivo. PLOS ONE. 2017;12:e0172838.

39. Anushiravani M, Bakhshaee M, Taghipour A, Naghedi-Baghdar H, Farshchi MK, Hoseini SS, et al. A systematic review of randomized controlled trials with herbal medicine on chronic rhinosinusitis. Phytother Res. 2017;32:395–401.

40. Massaro M, Piana S, Colletti CG, Noto R, Riela S, Baiamonte C, et al. Multicavity halloysite-amphiphilic cyclodextrin hybrids for co-delivery of natural drugs into thyroid cancer cells. J Mater Chem B. 2015;3:4074–81.

41. Dintcheva NT, Catalano G, Arrigo R, Morici E, Cavallaro G, Lazzara G, et al. Pluronic nanoparticles as anti-oxidant carriers for polymers. Polym Degrad Stab. 2016;134:194–201.

42. Ristić I, Krakovsky I, Janić T, Cakić S, Miletić A, Jotanović M, et al. The influence of the nanofiller on thermal properties of thermoplastic polyurethane elastomers. J Therm Anal Calorim. 2018;134:895–901.

43. Cicala G, Tosto C, Latteri A, La Rosa AD, Blanco I, Elsabbagh A, et al. Green Composites Based on Blends of Polypropylene with Liquid Wood Reinforced with Hemp Fibers: Thermomechanical Properties and the Effect of Recycling Cycles. Materials. 2017;10:998–1013.

44. Blanco I, Bottino FA. Thermal study on phenyl, hepta isobutyl-polyhedral oligomeric silsesquioxane/polystyrene nanocomposites. Polym Composite. 2013;34:225–32.

45. Rotaru A, Nicolaescu I, Rotaru P, Neaga C. Thermal characterization of humic acids and other components of raw coal. J Therm Anal Calorim. 2008;92:297–300.

46. Terekhova IV, Kulikov OV, Barannikov VP. Thermal dissociation of supramolecular complexes on the basis of 18-crown-6 and amino acids. Russ J Gen Chem. 2004;74:1213–7.

47. Sun P, Liu G, Lv D, Dong X, Wu J, Wang D. Effective activation of halloysite nanotubes by piranha solution for amine modification via silane coupling chemistry. RSC Adv. 2015;5:52916–25.

48. Rotaru A, Dumitru M. Thermal behaviour of CODA azoic dye liquid crystal and nanostructuring by drop cast and spin coating techniques. J Therm Anal Calorim. 2017;127:21–32.

49. Cavallaro G, Grillo I, Gradzielski M, Lazzara G. Structure of Hybrid Materials Based on Halloysite Nanotubes Filled with Anionic Surfactants. J Phys Chem C. 2016;120:13492–502.

Figure captions

Fig. 1 Photos of quercetin/fillers dispersions after equilibration (a). Percent of adsorbed quercetin as functions of the filler concentration (b).

Fig. 2 Linear fitting plots of Langmuir adsorption isotherms for quercetin/fillers mixtures.

Fig 3. Thermogravimetric curve for quercetin.

Fig. 4 Thermogravimetric curves for pristine fillers and quercetin/fillers composites.

Fig 5. Differential thermogravimetric curve for quercetin.

Fig 6. Differential thermogravimetric curves for quercetin/filler materials.

Fig. 1

Click here to access/download;Figure;Fig1.tif

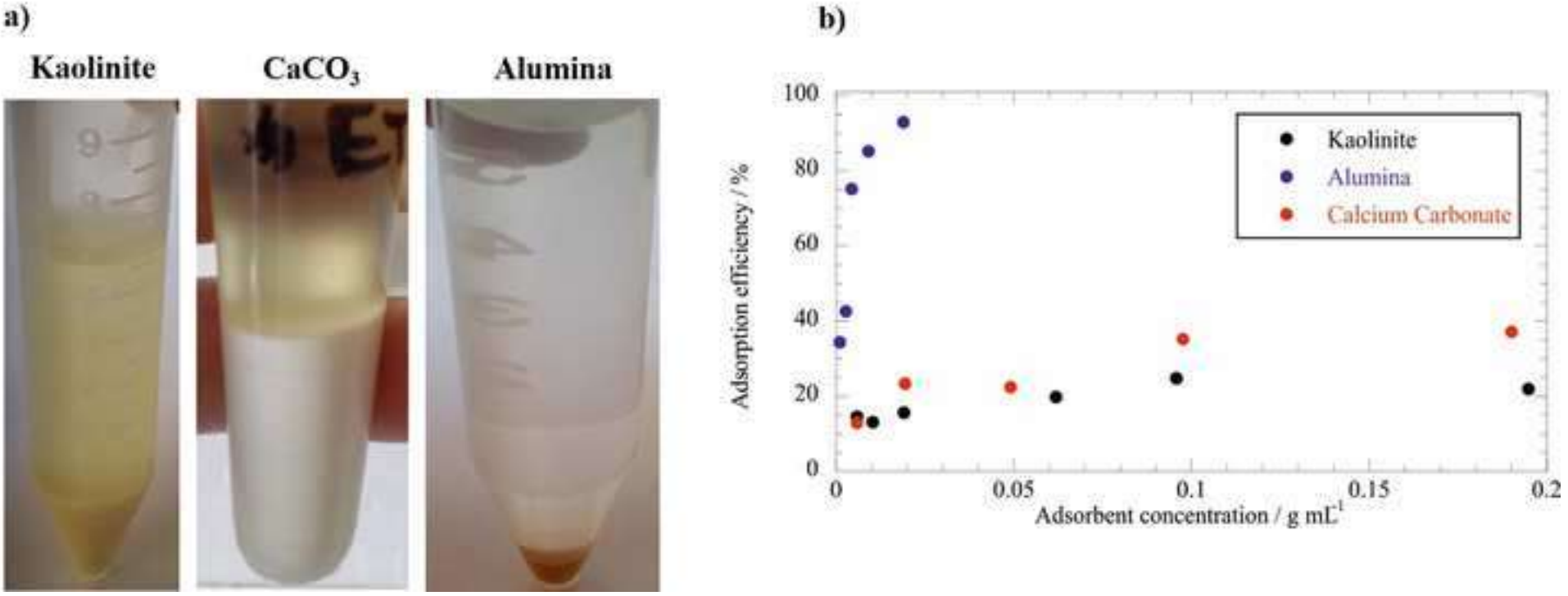

Fig. 2

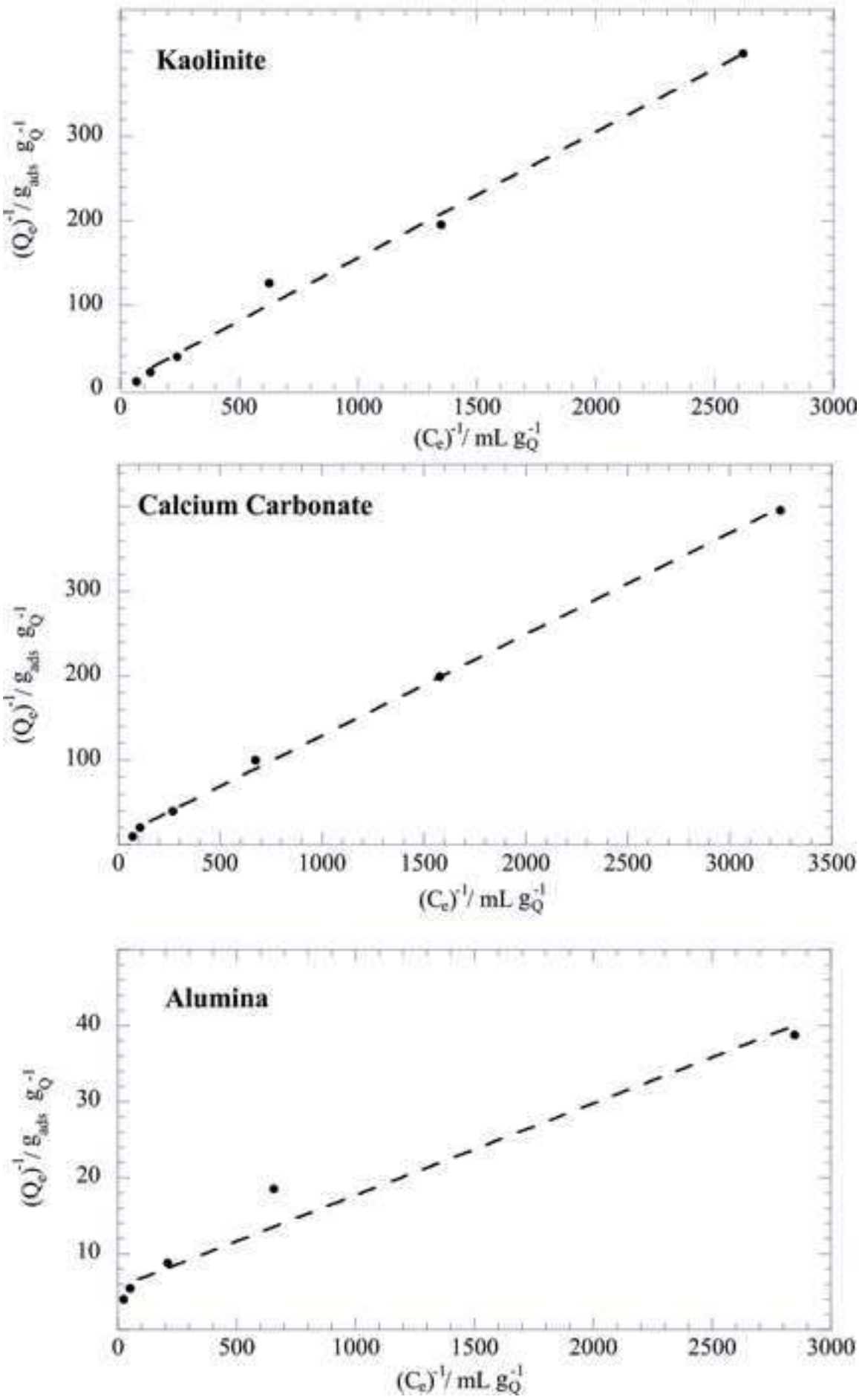

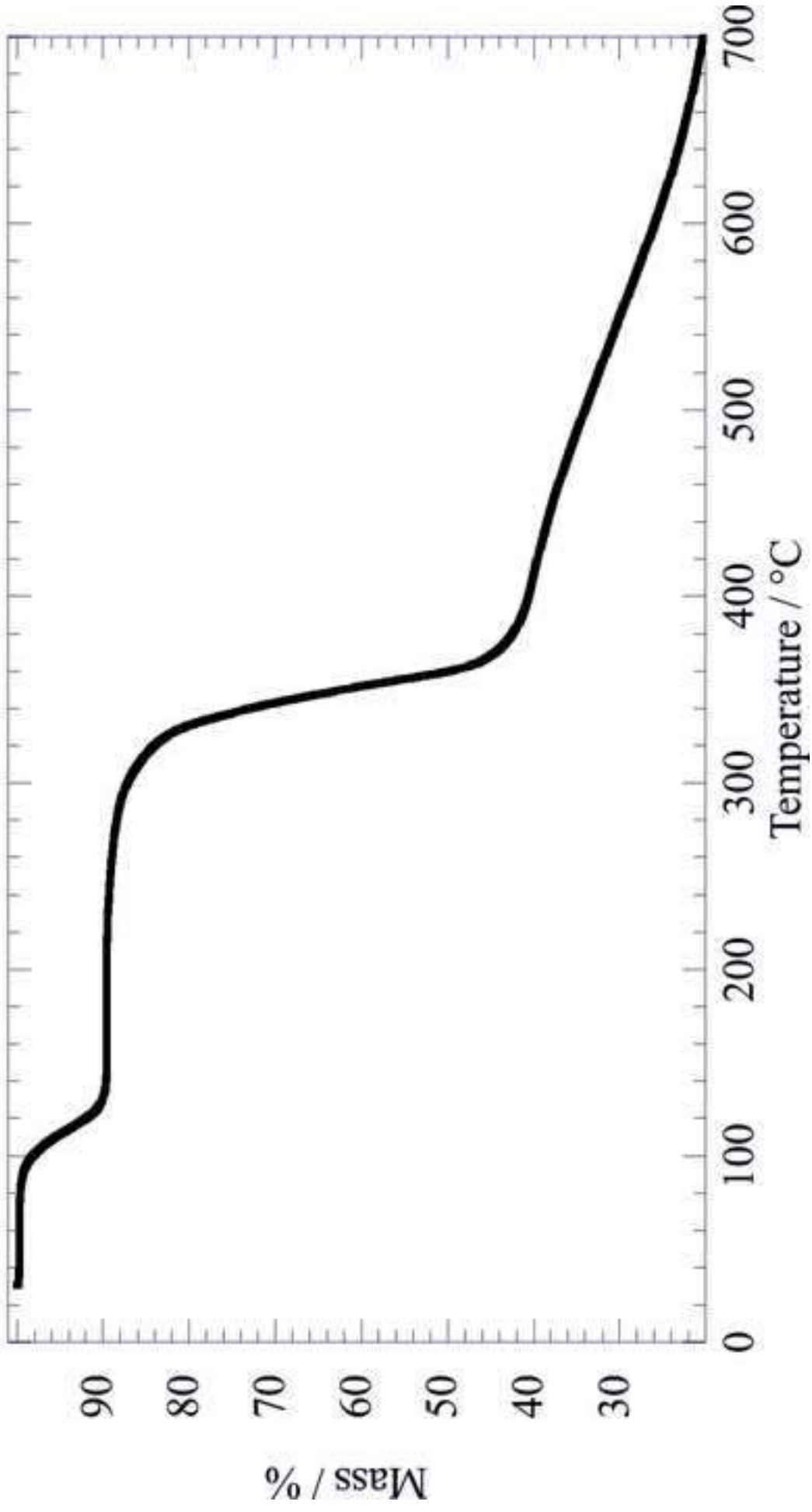

Fig. 3

Fig. 4

Click here to access/download;Figure;Fig4.tif

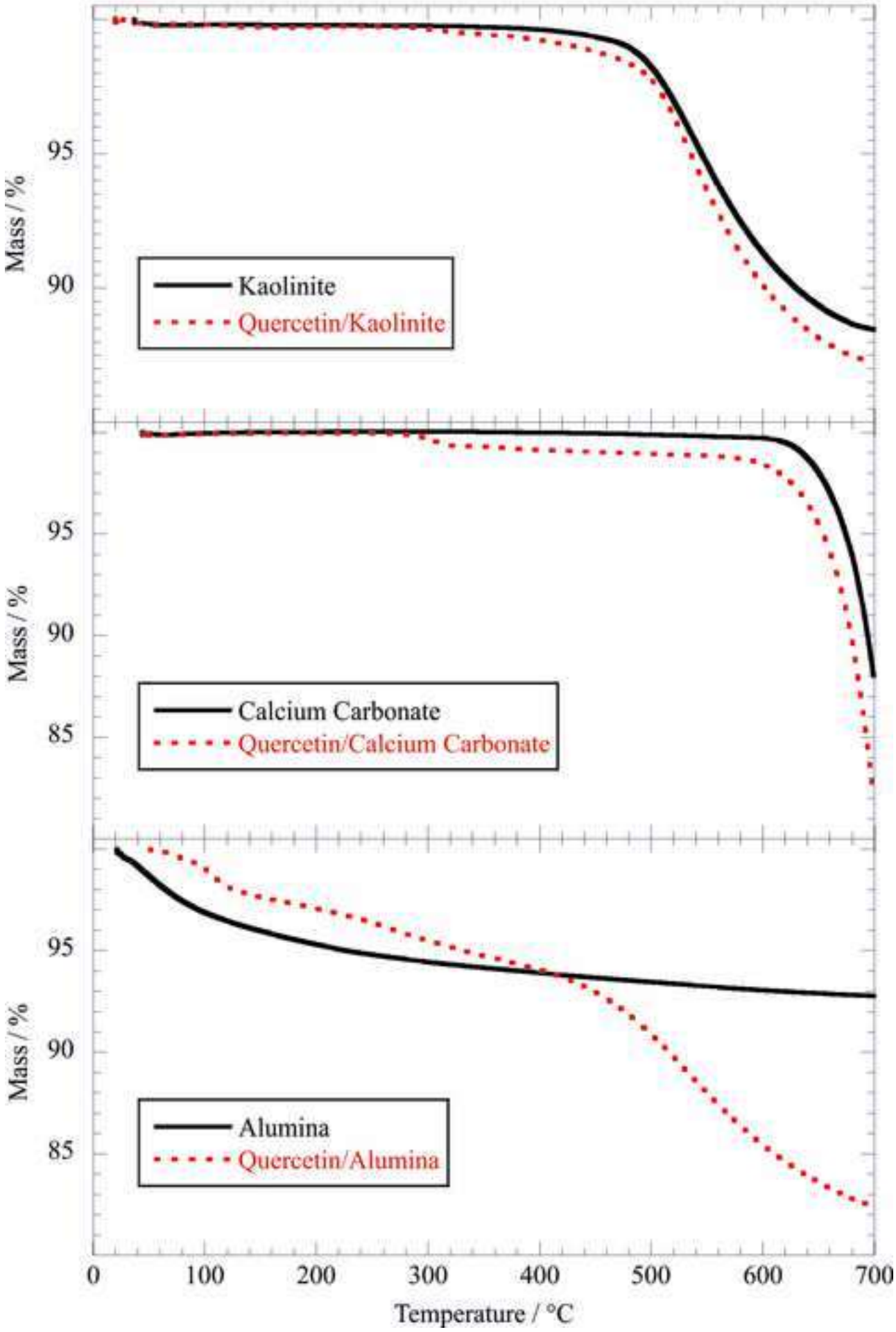

Fig. 5

Click here to access/download;Figure;Fig5.tif

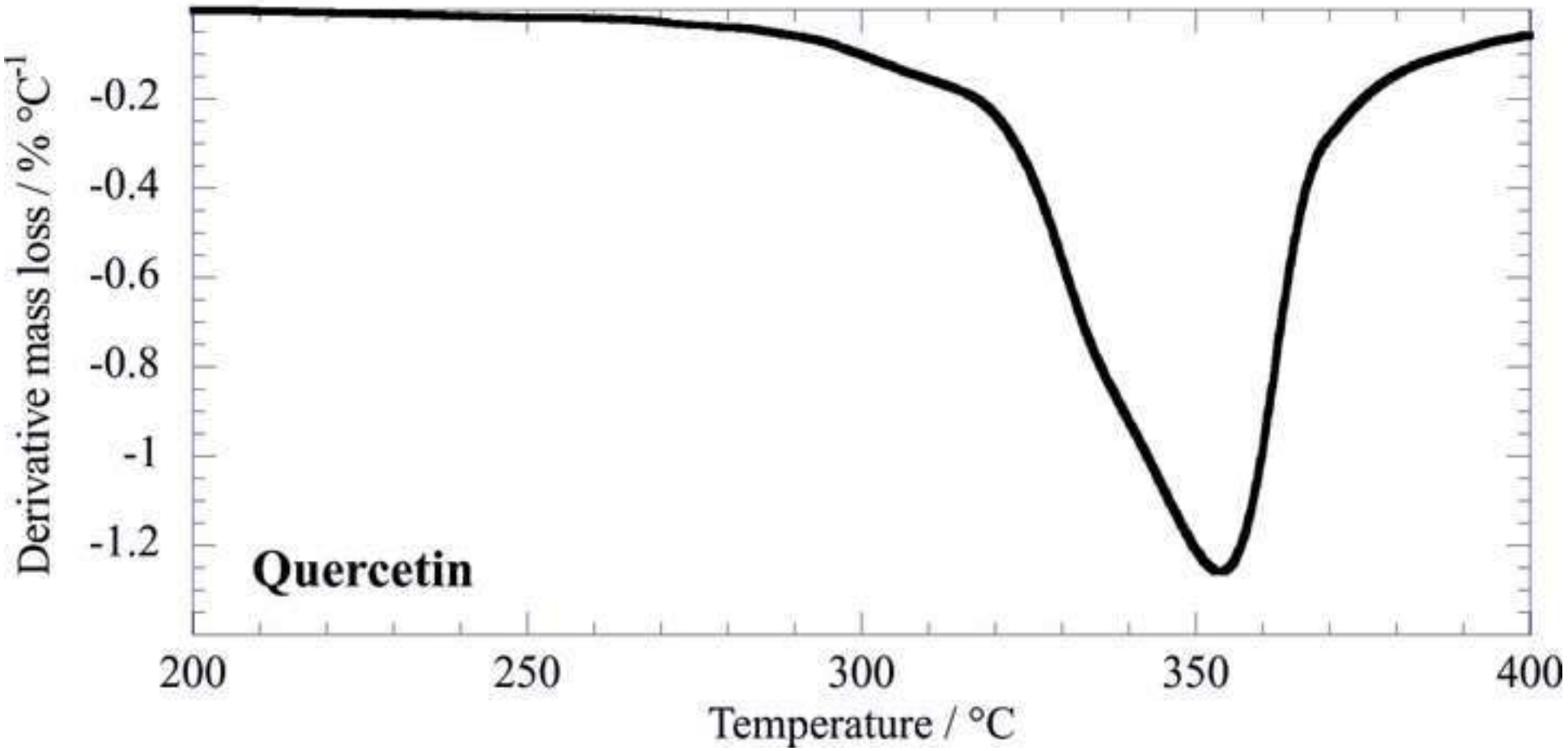

Fig. 6

Click here to access/download;Figure;Fig6.tif

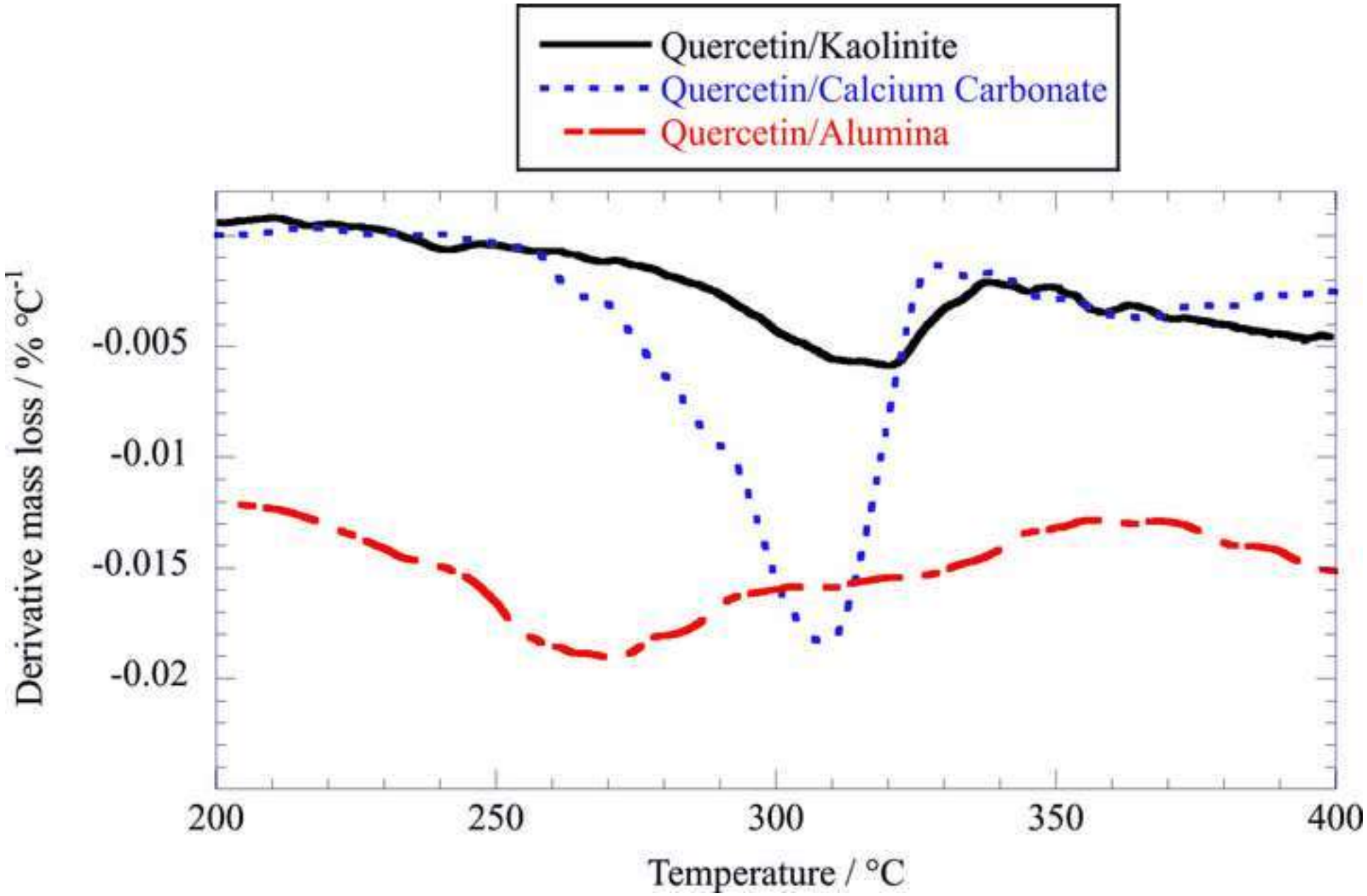

Table 1. Adsorption isotherm parameters obtained by the Langmuir model.

filler	Q_{max} / g_Q g_{ads}^{-1}	K_{ads} / mL g_Q^{-1}
Kaolinite	0.14 ± 0.03	46 ± 2
Calcium Carbonate	0.11 ± 0.04	75.1 ± 1.2
Alumina	0.18 ± 0.05	460 ± 60

Table 2. Quercetin loading determined by Thermogravimetry

filler	Loading / wt%
Kaolinite	1.53 ± 0.07
Calcium Carbonate	10.3 ± 0.5
Alumina	20.4 ± 1.2

Table 3. Quercetin degradation temperature determined from DTG peaks.

Material	Quercetin degradation temperature / °C
Quercetin	353.8
Quercetin/Kaolinite	320.0
Quercetin/Calcium Carbonate	308.9
Quercetin/Alumina	270.8